Two-Dimensional Small-Angle X-ray Scattering Investigation of Ionomer Deformation and Evaluation of Models of Ionomer Morphology

Susan A. Visser† and Stuart L. Cooper*

Department of Chemical Engineering, University of Wisconsin—Madison, Madison, Wisconsin 53706

Received July 2, 1991

ABSTRACT: The response to uniaxial extension of sulfonated model polyurethane ionomers based on PTMO soft segments was examined by small-angle X-ray scattering (SAXS). Ionomers based on 1000 molecular weight soft segments displayed highly nonaffine deformation behavior, whereas ionomers based on 2000 molecular weight soft segments underwent affine deformation up to elongation ratios of about 2. The SAXS data for the deformed ionomers were used to evaluate two models of ionomer morphology, one which attributes the observed scattering to interparticle interference and another which suggests the scattering arises from intraparticle interference. An interparticle interference model is shown to more accurately fit the data. To more fully explain the deformation results, a model of ionomer deformation is postulated in which an initial stage of aggregate rearrangement and subchain relaxation at low elongations is followed by subchain stretching at higher elongations.

I. Introduction

The precise arrangement of the ionic groups of ionomers in the relatively nonpolar polymer matrix remains open to speculation. While a few electron microscopy studies[1,2] have provided useful insight into ionomer morphology, the ionomer systems whose microstructures are amenable to study by electron microscopy are rare. Instead, ionomer morphology is typically probed using small-angle X-ray scattering (SAXS).

The typical SAXS pattern of ionomers is characterized by an upturn in intensity at low q, which has been attributed to an inhomogeneous distribution of ionic groups,[3,4] and a peak in scattered intensity, which is generally accepted as evidence of ionic aggregation. The broad peak and the absence of higher order scattering peaks make quantitative interpretation of ionomer SAXS patterns difficult. Quantitative interpretation often requires assumption of a morphological model to describe the observed scattering.

Two broad classes of morphological models have been proposed to interpret ionomer SAXS patterns, the intraparticle interference models[5-8] and the interparticle interference models.[9-12] The intraparticle interference models attribute the observed scattering behavior to short-range order within the ionic aggregates. The ionic aggregates are assumed to be dilute and randomly distributed in the matrix, leading to negligible interparticle scattering. In the interparticle interference models, the aggregates are assumed to be distributed in the matrix with some degree of order, leading to a scattering peak resulting from scattering between aggregates. Although experimental evidence in favor of the interparticle interference models is growing,[13-15] the intraparticle interference models have not been completely dismissed. Theoretical arguments[16] caused Dreyfus et al.[8] to propose a new interparticle interference model to interpret ionomer small-angle neutron scattering (SANS) data. Although evaluation of the model for use in analyzing ionomer SAXS data revealed that the model could not quantitatively reproduce the SAXS data,[9] experimental evidence[8] in favor of other intraparticle interference models suggests that further consideration is necessary.

One method of distinguishing between the two classes of morphological models is observation of the SAXS patterns of ionomers subject to deformation. Fujimara et al.[5,17] studied the deformation behavior of Nafion membranes using SAXS. On the basis of their uniaxial deformation results, the authors concluded that a core–shell or liquidlike hard-sphere model was better able to explain the data than a paracrystalline lattice model. The authors stressed, however, that more quantitative studies were needed to differentiate between the intraparticle (core–shell) and interparticle (liquidlike) interference models. SAXS studies of uniaxially deformed ethylene/methacrylic acid copolymers[6] also supported a core–shell model over a paracrystalline lattice model, but complete agreement between the core–shell model predictions and the experimental data was not obtained. Thus, further work is warranted.

In this paper, the response of model polyurethane ionomers to uniaxial deformation is probed with SAXS. The SAXS data are then used to quantitatively evaluate an intraparticle interference model, Fujimara's depleted-zone core–shell model,[5] and an interparticle interference model, Yarusso's liquidlike hard-sphere model.[10]

II. Experimental Section

A. Sample Preparation. The synthesis of the model polyurethane ionomers has been described previously.[26] The model polyurethane ionomers are 1:1 copolymers of a poly(tetramethylene oxide) (PTMO) soft segment and tolylene diisocyanate (TDI), which have sodium propyl sulfonate groups grafted solely at the urethane linkages. The chemical structure of the model polyurethane ionomers is shown in Figure 1. PTMO soft segments of M_n = 990 or 2070 were used. Samples were compression molded at 160 °C for 5 min at 10 kpsi and allowed to slowly cool to room temperature in the mold over a period of 1 h.

B. Sample Nomenclature. A Five-digit code was used to identify the ionomer samples. The first three letters indicate the soft-segment type (M = PTMO), the soft-segment molecular weight in thousands, and the sulfonate pendant anion. The final two letters are the chemical symbol for the neutralizing cation.

C. Small-Angle X-ray Scattering Measurements. The small-angle X-ray scattering (SAXS) data were obtained using

* Author to whom correspondence should be addressed.
† Present address: Eastman Kodak Company Research Laboratories, Rochester, NY 14650.

0024-9297/92/2225-2230$03.00/0

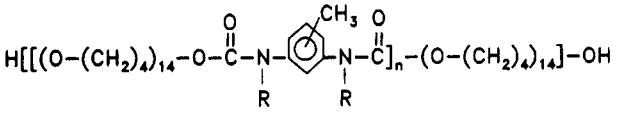

R = $-(CH_2)_3-SO_3Na^+$

Figure 1. Structure of the model polyurethane ionomer, using a 1000 molecular weight poly(tetramethylene oxide) (PTMO) polyol as an example. n is the overall degree of polymerization.

a Rigaku Cu rotating-anode point source, Charles Supper double-mirror-focusing optics, and a Nicolet two-dimensional detector. The scattering camera has a sample-to-detector distance of 46 cm. This configuration allowed a q ($q = (4\pi/\lambda)\sin\theta$, where 2θ is the scattering angle and λ is the wavelength of the radiation) range of 0.42 Å^{-1}, with a minimum q of 0.015 Å^{-1} due to the position of the beam stop, to be probed. Samples were uniaxially extended to elongation ratios $\lambda_b > 1$ ($\lambda_b = L/L_0$, where L_0 is the distance between two marks on the unstretched sample and L is the distance for the stretched sample) using a stretching jig placed in the X-ray path. Samples were stretched to the desired elongation ratio and allowed to relax in the new stretched configuration for at least 30 min prior to data collection. All data were collected at room temperature. The data were corrected for detector sensitivity, parasitic and background scattering, and absorption of X-rays by the sample.

III. Models of Ionomer Morphology

A. Depleted-Zone Core-Shell Model. The depleted-zone core–shell (DZCS) model of Fujimara et al.[5] was proposed as a modification of the core–shell model of MacKnight and co-workers.[7] In the DZCS model, pictured schematically in Figure 2, electrostatic attractions drive ionic aggregation to form core–shell particles with a core radius R_1 and an outer shell radius R_2. When the ionic groups aggregate to form clusters, regions of the matrix surrounding the core are depleted of the ionic groups which went to form the cluster, leading to a structure with three electron densities: the matrix electron density ρ_0, which reflects both the backbone-chain electron density and the electron density of the ionic groups dispersed in the matrix; the depleted-zone (shell) electron density ρ_2; and the ionic core electron density ρ_1. A preferred distance separating the core and the matrix is established by the clustering process; this gives rise to the peak in the scattered intensity.

The scattered intensity of the DZCS model is given by[5]

$$\frac{I}{I_e V} = \frac{16\Pi^2}{9\nu_P}[(\rho_1 - \rho_2)R_1^3\phi(u_1) + (\rho_2 - \rho_0)R_2^3\phi(u_2)]^2 \qquad (1)$$

where I_e is the scattering from a single electron, V is the scattering volume, ν_P is the average sample volume per particle, and for spheres of constant density[18]

$$\phi(u_i) = 3\frac{\sin u_i - u_i \cos u_i}{u_i^3} \qquad u_i = qR_i \qquad (2)$$

By assuming that the core–shell particle is deformed affinely with a constant volume into an ellipsoidal core–shell, Fujimara et al.[5] have shown that the scattered intensity from the deformed shell particle is given by replacing u_i in eq 2 with u_i^*

$$u_i^* = u_i\lambda_b^{-1/2}[1 + (\nu^2 - 1)\cos^2\theta\cos^2\mu]^{1/2} \qquad (3)$$

with ν as the axial ratio of the ellipsoidal particles, related to the bulk elongation ratio λ_b by

$$\nu^2 = \lambda_b^3 \qquad (4)$$

and μ is the azimuthal angle. ($\mu = 0°$ specifies the intensity distribution along the meridian, i.e., parallel to the stretching direction.)

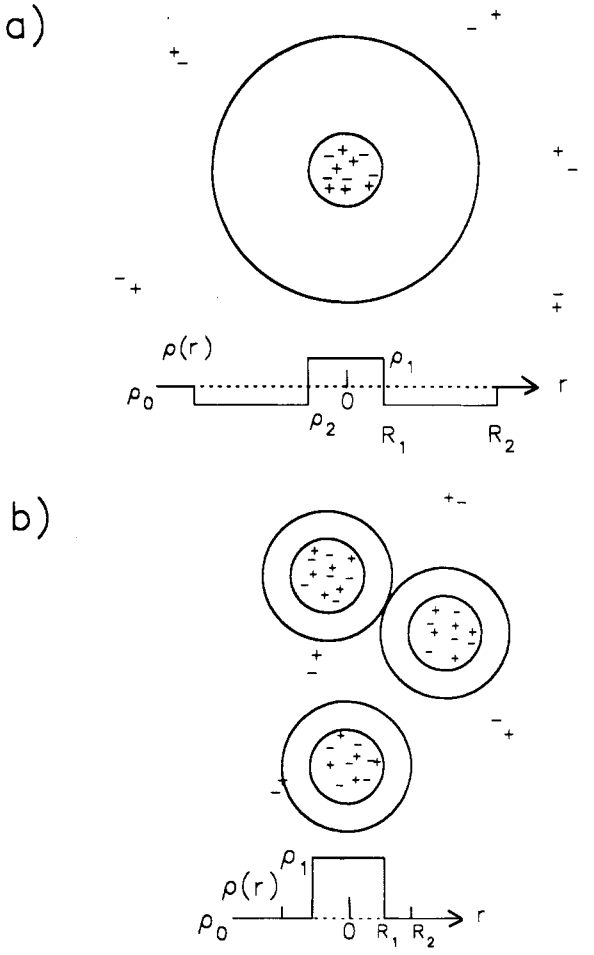

Figure 2. Schematic representations of the (a) depleted-zone core–shell model and (b) the liquidlike hard-sphere model.

B. Liquidlike Hard-Sphere Model. The liquidlike hard-sphere (LLHS) model postulated by Yarusso and Cooper[10] assumes that ionic aggregates are hard spheres distributed with a liquidlike degree of order in the amorphous matrix. The ionic aggregates are modeled as spheres of radius R_1 and electron density ρ_1 which are surrounded by an impenetrable polymer sheath of electron density equal to that of the matrix (ρ_0) to give a radius of closest approach $R_2 > R_1$, as pictured in Figure 2. The polymer sheath arises from the connectivity of the polymer chains and the ionic groups. Unlike the DZCS model, the scattering here is postulated to arise from interparticle interference between the aggregates.

The equation describing the scattered intensity from the LLHS model, modified to include the Percus–Yevick total correlation function, is[9]

$$\frac{I}{I_e V} = \frac{1}{\nu_P}\left[\frac{4\pi R_1^3}{3}\right]^2(\rho_1 - \rho_0)^2\phi^2(u_1)\,S(2u_2) \qquad (5)$$

where ϕ is given by eq 2, ν_P is the volume of material per ionic aggregate (the inverse of the aggregate number density), and $S(2u_2)$ is the interference function, which has been given in the Percus–Yevick form previously.[19]

For the case of uniaxially deformed samples, it is assumed that the vectors connecting the scattering centers are affinely deformed with constant volume. Hard-sphere repulsion represents the only possible form of physical interaction between the spheres. The spheres are assumed to be monodisperse, and the particles are assumed to

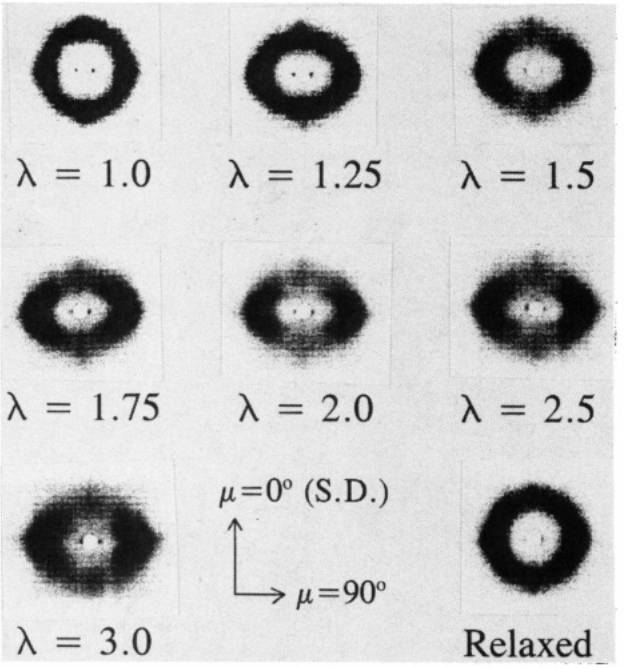

Figure 3. Two-dimensional SAXS patterns for M1SNa at various elongation ratios.

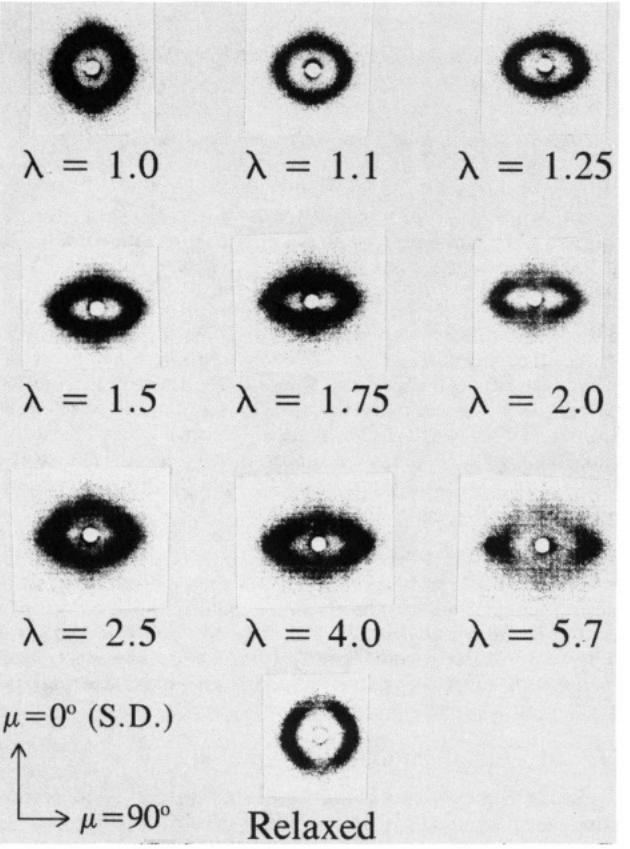

Figure 4. Two-dimensional SAXS patterns for M2SNa at various elongation ratios.

deform affinely under constant volume. Under these conditions, the scattering intensity can be derived following Fujimara.[5] Then, the scattering intensity of the deformed sample is given by replacing u_i in eq 5 by u_i^*

$$u_i^* = u_i \lambda_b^{-1/2}[1 + (\lambda_b^3 - 1)\cos^2\theta\cos^2\mu]^{1/2} \quad (6)$$

where u_i is given by eq 3, R_i being the radius of the hard spheres in the undeformed state. (Details of the derivation precisely follow ref 5.)

IV. Results and Discussion

Figure 3 shows the two-dimensional SAXS patterns for M1SNa ionomers which were allowed to relax in their stretched conformation prior to data collection. In its unstressed state ($\lambda_b = 1$), the M1SNa ionomer gives a fully isotropic, circular two-dimensional SAXS pattern which corresponds to the single broad peak apparent in the one-dimensional SAXS patterns discussed previously.[9] Upon mild extension to $\lambda_b = 1.25$, the SAXS pattern is transformed to an ellipsoidal shape characteristic of the anisotropy induced by stretching. The meridional maximum ($\mu = 0°$) shifts toward smaller q, but the equatorial ($\mu = 90°$) maximum shifts toward larger q. While difficult to discern in Figure 3, the onset of anisotropy is accompanied by not only a change in the shape of the scattering pattern but also a change in the intensity distribution. The scattered intensity of the deformed samples is greatest in the equatorial direction and falls off as the meridional direction is approached. At higher values of λ_b, the ellipsoidal nature of the scattering pattern becomes slightly more pronounced, but the scattered intensity distribution remains approximately constant, with the equatorial intensity maximum remaining noticeably greater than the meridional intensity maximum.

In order to test the reversibility of the deformation process, the M1SNa sample was allowed to relax overnight without external application of stress after the data were collected at $\lambda_b = 3.0$. The scattering pattern of the "relaxed" specimen is also shown in Figure 3. The scattering pattern of the relaxed sample is nearly identical to that of the sample at $\lambda_b = 1$, prior to the start of deformation. This indicates not only that the deformation process is almost completely reversible but also that wholesale morphological rearrangement during the stretching process is unlikely. (The ionomer returned to within 10% of its unstretched length within 10 min after its release from the stretching device, indicating that long-time morphological rearrangements are unlikely to have occurred prior to collection of the relaxed SAXS pattern.) Previous infrared dichroism results for M1SNa[20] indicated a high degree of cohesiveness in the ionic aggregates, leading to a lower degree of ion-hopping (transport of ionic groups between ionic aggregates[21-23]). The highly cohesive ionic aggregates tend to act more as chemical than as physical cross-links, allowing reversibility in the deformation/relaxation process. Thus, the SAXS data support the cohesive nature of the ionic aggregates and the low degree of ion-hopping expected in this ionomer.

The two-dimensional SAXS patterns for M2SNa are shown in Figure 4. Again, the pattern at $\lambda_b = 1$ is circular, with no higher order reflections, indicating the isotropic nature of the unstretched sample's morphology and matching well the previous one-dimensional SAXS result.[9] Upon stretching, the meridional scattering maximum ($\mu = 0°$) shifts to lower q, while the equatorial maximum ($\mu = 90°$) shifts toward higher q. Compared to the deformation behavior of M1SNa, the shifts in the M2SNa patterns are more pronounced, giving a higher eccentricity to the ellipsoidal patterns for M2SNa. This also corresponds well to previous infrared dichroism data,[20] which indicated a higher degree of orientability of the matrix (PTMO) material in M2SNa than in M1SNa.

The recovery of the M2SNa ionomer from deformation is also less complete than that of the M1SNa sample. While the circular shape of the SAXS pattern has been reattained, the equatorial scattering intensity still remains

Table I
Model Fit Parameters for Unstretched Samples

	depleted-zone core–shell model				liquidlike hard-sphere model		
sample	R_1, Å	R_2, Å	$\rho_1 - \rho_2$, e/Å^3	$\rho_2 - \rho_0$, e/Å^3	R_1, Å	R_2, Å	ν_P, nm^3
M1SNa	15.92	39.14	0.1954	−0.0211	13.61	22.52	169.2
M2SNa	27.91	40.43	0.1726	−0.0442	16.23	29.32	401.1

greater than the meridional intensity. Although this may result from a greater orientability of the PTMO matrix in M2SNa than in M1SNa, it could also result from the higher maximum extension ratio to which M2SNa was stretched or from the onset of stress crystallization in M2SNa at higher elongations. PTMO(2000)-based polyurethanes[24] and polyurethane ionomers[25] can exhibit crystallinity in the unstressed state, and previous work on M1SNa and M2SNa samples cast from solution indicates the onset of stress crystallization at values of λ_b = 5.0 and 5.3, respectively.[26] A compression-molded M1SNa sample began stress crystallization at λ_b = 4.1, still much greater than the elongation examined here. Thus, no definitive conclusion can be drawn other than extensive but incomplete recovery of the initial morphology.

In order to quantitatively analyze the ability of the two models discussed in section III to predict the deformation results, the SAXS data at λ_b = 1 were fit with each model. Model fit parameters appear in Table I. (Note that the absence of data in absolute intensity units will affect the values of the model parameters slightly.) As the SAXS data are not on an absolute intensity scale and corrections could not be made for fluctuations in source intensity from one scattering pattern to the next, intensity maxima at different values of λ_b cannot be compared. However, the intensities at μ = 0° and μ = 90° at any given elongation can be compared and should give an accurate assessment of how scattered intensity varies with the azimuthal angle. Accordingly, in order to present model fits for the scattering patterns, the parameters in Table I were fixed and ν_P, for the DZCS model, or $\Delta\rho$, for the LLHS model, were allowed to vary to provide the best fit to the equatorial (μ = 90°) scattering data. (These data were selected for fitting because of their higher intensity and presumably higher signal-to-noise ratio.) Following calculation of the optimum values of ν_P or $\Delta\rho$ by a nonlinear least-squares fitting method and addition of a constant background term, all parameters were fixed, and the scattering patterns for μ = 0° were calculated. The experimental data and model fits are shown in Figures 5–8.

The model fits for the equatorial scattering (μ = 90°) for M1SNa are in reasonable agreement with experimental data up to λ_b = 1.5. At higher elongations, however, both models yield a larger shift in peak position than is observed in the data. Although both model fits result in identical peak shifts in the equatorial scattering, the peak shape given by the LLHS model more closely matches the experimental data than that found for the DZCS model.

Examination of the meridional scattering, however, shows that, even at low extension ratios, the models give poor fits to the data. For the DZCS model, the level of the intensity maximum is independent of μ, whereas the data show that the intensity decreases with μ at any given value of $\lambda_b > 1$. Postulating an inhomogeneous deformation of the core–shell particles could account for some of the decrease in the intensity with μ. If the deformation resulted in destruction of the core–shell structure in the direction parallel to the stretching direction, a loss of short-range order distance would occur. This inhomogeneous deformation mechanism could result in the peak broadening and intensity loss at μ = 0°. However, the fact that

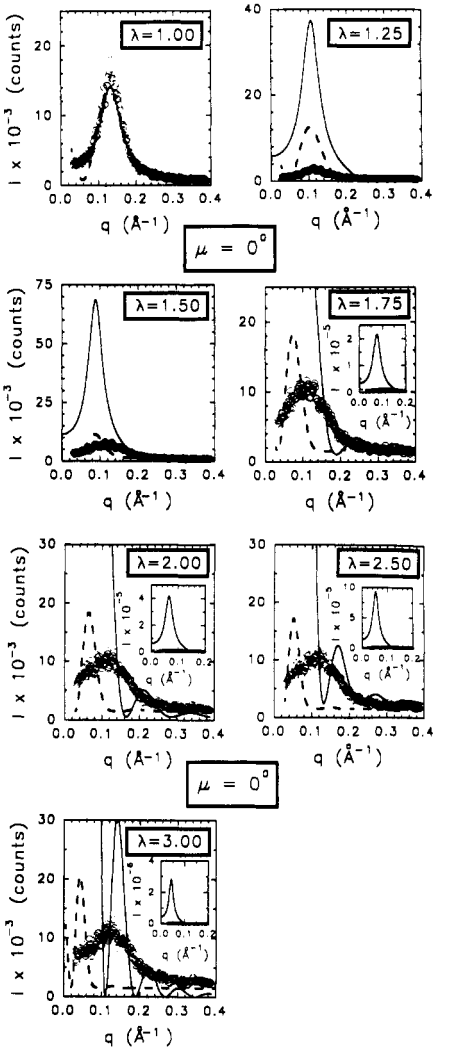

Figure 5. Comparisons of meridional (azimuthal angle μ = 0°) scattering data and model fits for M1SNa at various elongation ratios: (O) experimental data; (—) LLHS model fit; (- - -) DZCS model fit.

M1SNa recovers almost completely upon removal of the stress makes a destructive mechanism unlikely. Also, the failure of the DZCS model to match the peak position even at very low elongations brings the usefulness of this model into question.

In contrast, the LLHS model fits of the data yield a change in the scattering intensity with μ. However, the change is in increasing intensity with decreasing μ, whereas the data show the opposite. The peak position predicted by the LLHS model matches the data at low elongations ($\lambda_b \leq 1.5$) more closely than the DZCS model, and postulation of polydispersity in the size of the hard spheres in the LLHS model could account for some of the discrepancy between predicted and actual intensity values.

At higher elongations, the agreement between either of the models and the data is extremely poor. Neither peak shape, peak position, nor peak intensity in the meridional scattering is accurately predicted by the DZCS or the LLHS model. The possibility of nonaffine deformation

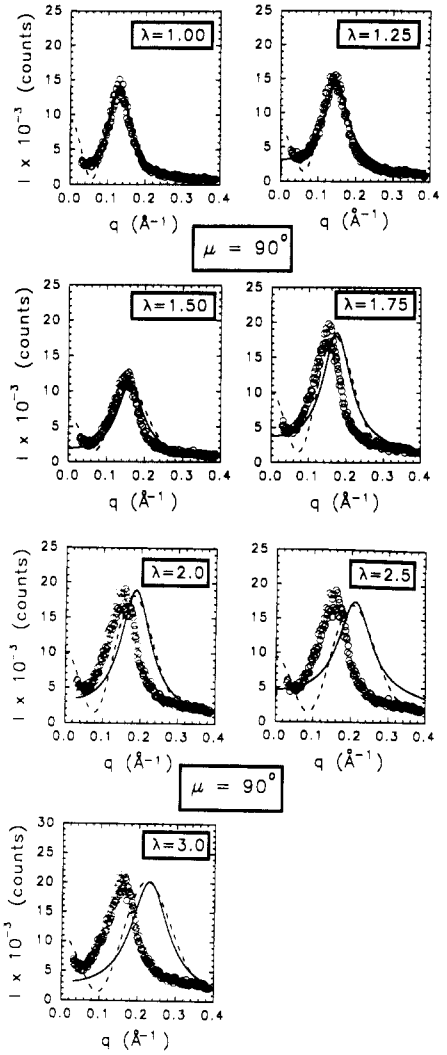

Figure 6. Comparisons of equatorial (azimuthal angle $\mu = 90°$) scattering data and model fits for M1SNa at various elongation ratios: (O) experimental data; (—) LLHS model fit; (- - -) DZCS model fit.

and volume dilation upon extension makes it difficult to condemn both models based on the high λ_b results, however.

For the M2SNa ionomer, there is relatively good agreement between the predictions of the DZCS model and the experimental data at $\mu = 0°$ and $\mu = 90°$ up to an elongation ratio of $\lambda_b = 1.75$. In contrast, the LLHS model again overpredicts the intensity of the $\mu = 0°$ scattering. At higher elongations, both models overpredict the shift in peak position to higher q at $\mu = 90°$ or to lower q at $\mu = 0°$.

The peak positions of the SAXS data for M1SNa and M2SNa can be used to calculate Bragg spacings (d) and microscopic elongation ratios $\lambda_d = d/d_0$, where d is the stretched-sample spacing and d_0 is the unstretched-sample spacing. (It should be noted that Bragg spacings are proportional to, but not a precise measure of, interaggregate distances.) Comparisons of the microscopic and bulk extension ratios are shown in Figures 9 and 10. At low elongations ($\lambda_b < 2$), the Bragg peak of the M2SNa sample undergoes affine deformation. This does not occur for M1SNa and may result from the greater orientability of the M2SNa matrix.[20] At higher values of λ_b, neither M1SNa nor M2SNa undergoes affine deformation under constant volume.

If an interparticle interference model is correct, λ_d should be close to λ_b. Having λ_d less than the affine deformation

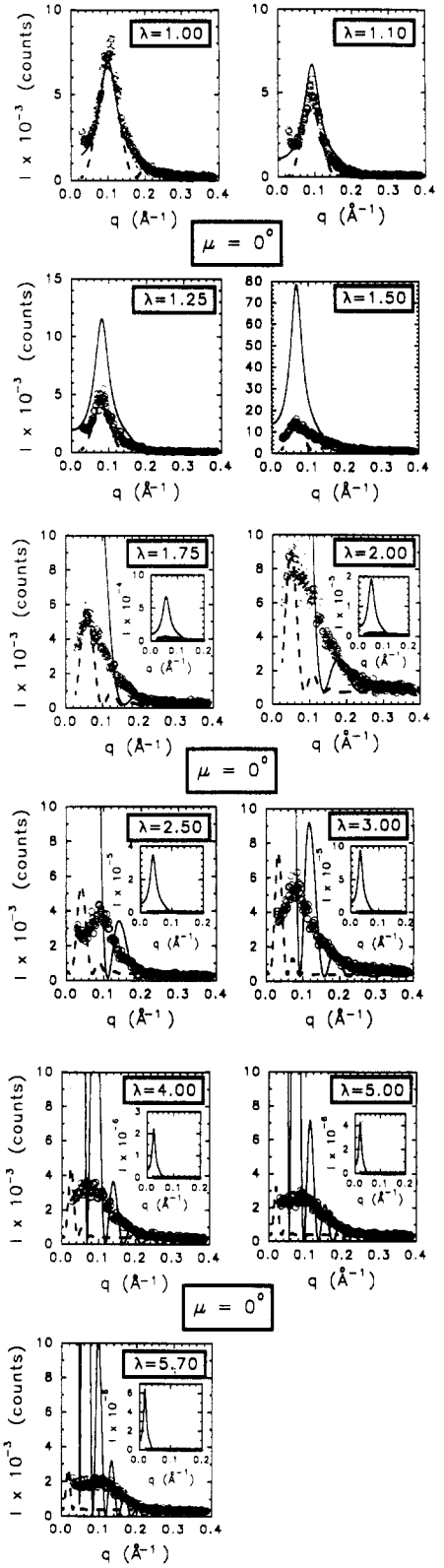

Figure 7. Comparisons of meridional (azimuthal angle $\mu = 0°$) scattering data and model fits for M2SNa at various elongation ratios: (O) experimental data; (—) LLHS model fit; (- - -) DZCS model fit.

prediction can only be explained with an interparticle interference model if the deformation is very inhomogeneous. Recent small-angle neutron scattering (SANS) experiments on uniaxially extended M1SNa and M2SNa ionomers,[27] taken in concert with the SAXS results presented here, suggest that this is the case. The SANS results showed no change in PTMO subchain dimensions

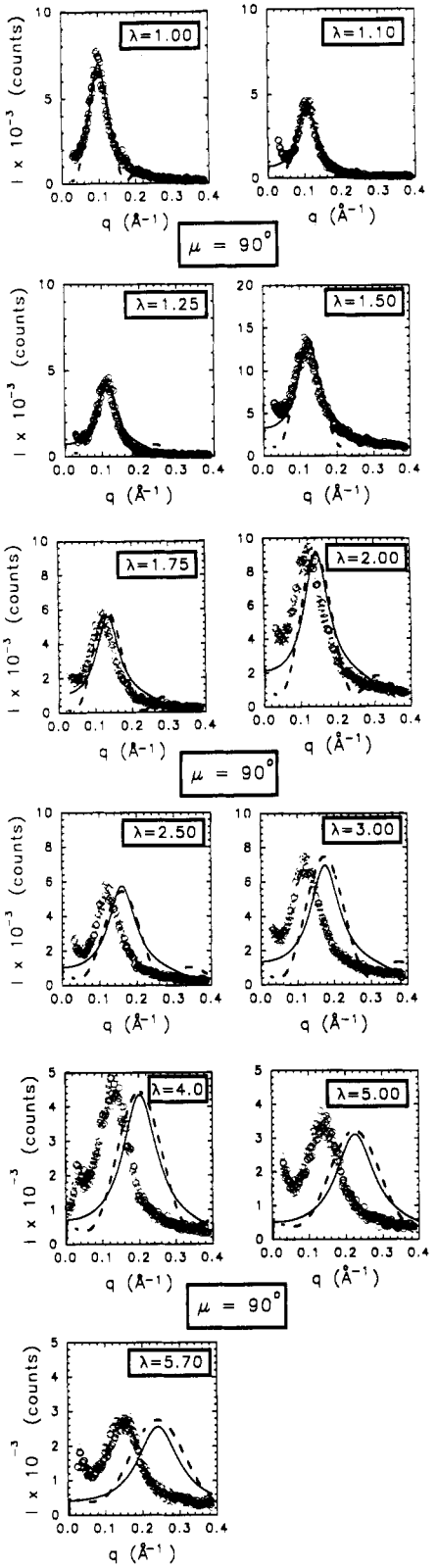

Figure 8. Comparisons of equatorial (azimuthal angle $\mu = 90°$) scattering data and model fits for M2SNa at various elongation ratios: (O) experimental data; (—) LLHS model fit; (- - -) DZCS model fit.

up to $\lambda_b = 1.75$ for M1SNa, while the peak positions parallel and perpendicular to the stretching direction changed noticeably in the SAXS patterns. At higher elongations ($\lambda \geq 1.75$), anisotropy was apparent in the SANS patterns, indicating chain stretching, while the SAXS peak position in the directions parallel and perpendicular to the stretching direction remained approximately constant.

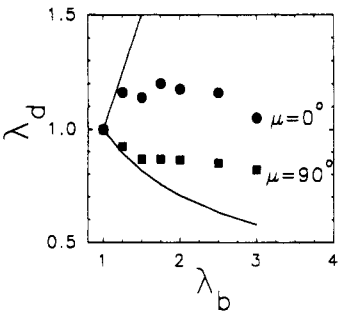

Figure 9. Change of the microscopic elongation ratio (λ_d) with the macroscopic deformation ratio (λ_b) for an M1SNa ionomer. Symbols indicate experimental values calculated from a simple Bragg spacing analysis; solid lines are predictions based on affine deformation.

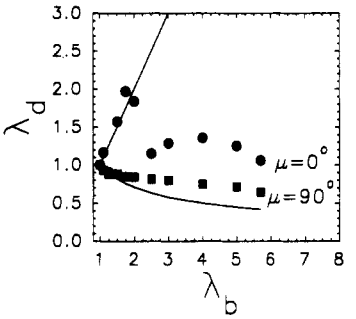

Figure 10. Change of the microscopic elongation ratio (λ_d) with the macroscopic deformation ratio (λ_b) for an M2SNa ionomer. Symbols indicate experimental values calculated from a simple Bragg spacing analysis; solid lines are predictions based on affine deformation.

These results suggest the following response of the ionomers to deformation. At low elongations, the deformation is characterized by rearrangement of the ionic aggregates in the polymer matrix, allowing a relaxation of the PTMO subchains and the observation of isotropic single-chain SANS patterns. The rearrangement of the ionic aggregates at low λ_b also results in a shift in the SAXS peak position; therefore, the SAXS peak must arise from interparticle interference. At higher elongations, aggregate rearrangement is unable to allow complete subchain relaxation, and chain stretching occurs. This deformation mechanism is also supported by the M2SNa data. The SAXS peak position for M2SNa changes in q space up to $\lambda_b = 2.0$, precisely the elongation at which anisotropy becomes apparent in the SANS data. An initial stage of aggregate rearrangement, followed by chain stretching at higher elongations, explains the M2SNa scattering results.

An interparticle interference model also explains the change in the scattered intensity distribution with the azimuthal angle in the stretched samples. As the sample is stretched, the interdomain spacing in the stretching direction increases, causing the liquidlike ordering of the aggregates to begin to be lost. Evidence for changes in aggregate ordering with elongation has been seen in the SAXS results of other uniaxially extended model polyurethane ionomers.[28] As the liquidlike ordering is lost, the intensity of the meridional scattering decreases relative to the equatorial scattering, where the spacing remains relatively constant. Loss of the liquidlike ordering also explains the failure of the LLHS model to fit the entire range of experimental data.

The scattering data rule out a core–shell model. For a core–shell model, λ_d is associated with the short-range order distance. Therefore, if λ_d is less than λ_b, the deformation of the core–shell particle would have to be

less than the matrix deformation. The SANS results show that the matrix chains remain undeformed at low elongations; the core–shell particle would also have to remain undeformed if the core–shell model were to be applied. In this case, however, the shift in SAXS peak position could not be reproduced by the model. Thus, the model is inconsistent with the available data.

V. Conclusions

The deformation response of two sulfonated model polyurethane ionomers was examined by SAXS. Elongation of the ionomers was shown to transform the initially circular, isotropic SAXS patterns to ellipsoidal patterns whose scattered intensity maxima were dependent on the azimuthal angle. Differences in the responses of M1SNa and M2SNa were attributed to the orientability of their PTMO matrices. Both ionomers were seen to recover nearly all the morphological characteristics of the unstretched samples, as observable by SAXS, after the samples were allowed to relax from the stretched state.

An interparticle interference model, Yarusso and Cooper's liquidlike hard-sphere (LLHS) model,[10] and an intraparticle interference model, the depleted-zone core–shell (DZCS) model of Fujimara et al.,[5] were evaluated for their ability to predict ionomer deformation behavior. Under assumptions of affine deformation of the matrix and the ionic particles, both models gave reasonable fits to the equatorial scattering at low elongations, but both models failed to accurately predict the lowering of the scattered intensity in the meridional direction for M1SNa. For M1SNa and M2SNa at higher elongations, the overall agreement between either model and the data was poor.

The SAXS results indicate that the deformation of M1SNa is highly nonaffine and the deformation of M2SNa is affine only at low elongations. SANS results on the same systems[27] indicated that deformation was inhomogeneous. Considering the SAXS and SANS results together, a model of ionomer deformation comprising an initial stage of aggregate rearrangement, followed by chain stretching at higher elongations, was proposed. The data and model both confirmed the validity of an interparticle interference model for describing ionomer SAXS results and ruled out an intraparticle interference model.

The discrepancies between the LLHS model fit, and the SAXS data were attributed partially to changes in the ordering of the ionic aggregates upon elongation. The noaffine nature of the deformation should also be considered in formulating any new models for describing the deformation behavior of these ionomers. The LLHS model is still expected to accurately model the scattering peak of many undeformed ionomers, although postulation of another source of scattering, such as that arising from the two-phase morphology suggested by Eisenberg,[29] may be necessary to fit the complete scattering pattern.

Acknowledgment. A special thanks goes to Prof. R. E. Cohen and Dr. Kostas Douzinas for their assistance in collection of the small-angle X-ray scattering data presented in this paper. Support for this work was provided by the U.S. Department of Energy through Grant DE-FG02-88ER45370 and by the donors of the Petroleum Research Fund, administered by the American Chemical Society. S.A.V. gratefully acknowledges the fellowship support of the American Association of University Women Educational Fund in the form of an Engineering Dissertation Fellowship.

References and Notes

(1) Li, C.; Register, R. A.; Cooper, S. L. *Polymer* **1989**, *30*, 1227.
(2) Williams, C. E.; Colliex, C.; Horrion, J.; Jerome, R. In *Multiphase Polymers: Blends and Ionomers*; Utracki, L. A., Weiss, R. A., Eds.; ACS Symposium Series 395; American Chemical Society: Washington, DC, 1989; p 439.
(3) Register, R. A.; Cooper, S. L. *Macromolecules* **1990**, *23*, 310.
(4) Register, R. A.; Cooper, S. L. *Macromolecules* **1990**, *23*, 318.
(5) Fujimara, M.; Hashimoto, T.; Kawai, H. *Macromolecules* **1982**, *15*, 136.
(6) Roche, E. J.; Stein, R. S.; Russell, T. P.; MacKnight, W. J. *J. Polym. Sci., Polym. Phys. Ed.* **1980**, *18*, 1497.
(7) MacKnight, W. J.; Taggart, W. P.; Stein, R. S. *J. Polym. Sci., Polym. Symp.* **1974**, *45*, 113.
(8) Dreyfus, B.; Gebel, G.; Aldebert, P.; Pineri, M.; Escombes, M.; Thomas, M. *J. Phys. Fr.* **1990**, *51*, 1341.
(9) Visser, S. A.; Cooper, S. L. *Macromolecules* **1991**, *24*, 2584.
(10) Yarusso, D. J.; Cooper, S. L. *Macromolecules* **1983**, *16*, 1871.
(11) Lee, D. C.; Register, R. A.; Yang, C. Z.; Cooper, S. L. *Macromolecules* **1988**, *21*, 998.
(12) Marx, C. L.; Caulfield, D. F.; Cooper, S. L. *Macromolecules* **1973**, *6*, 344.
(13) Williams, C. E.; Russell, T. P.; Jerome, R.; Horrion, J. *Macromolecules* **1986**, *19*, 2877.
(14) Register, R. A.; Pruckmayr, G.; Cooper, S. L. *Macromolecules* **1990**, *23*, 3023.
(15) Yarusso, D. J.; Cooper, S. L. *Polymer* **1985**, *26*, 371.
(16) Dreyfus, B. *Macromolecules* **1985**, *18*, 284.
(17) Fujimara, M.; Hashimoto, T.; Kawai, H. *Macromolecules* **1981**, *14*, 1309.
(18) Rayleigh, L. *Proc. R. Soc. (London)* **1914**, *A90*, 219.
(19) Ding, Y. S.; Register, R. A.; Yang, C. Z.; Cooper, S. L. *Polymer* **1989**, *30*, 1213.
(20) Ding, Y. S.; Register, R. A.; Yang, C. Z.; Cooper, S. L. *Polymer* **1989**, *30*, 1204.
(21) Ward, T. C.; Tobolsky, A. V. *J. Appl. Polym. Sci.* **1967**, *11*, 2403.
(22) Sakamoto, K.; MacKnight, W. J.; Porter, R. S. *J. Polym. Sci., Polym. Phys. Ed.* **1974**, *8*, 277.
(23) Hara, M.; Eisenberg, A.; Storey, R. F.; Kennedy, J. P. In *Coulombic Interactions in Macromolecular Systems*; Eisenberg, A., Bailey, F. E., Eds.; ACS Symposium Series 302; American Chemical Society: Washington, DC, 1986; p 176.
(24) Vallance, M. A.; Castles, J. L.; Cooper, S. L. *Polymer* **1984**, *25*, 1734.
(25) Lee, D. C.; Register, R. A.; Yang, C. Z.; Cooper, S. L. *Macromolecules* **1988**, *21*, 1005.
(26) Visser, S. A.; Cooper, S. L. *Macromolecules* **1991**, *24*, 2576.
(27) Visser, S. A.; Cooper, S. L. Submitted to *Polymer*, June 1991.
(28) Visser, S. A.; Cooper, S. L. Submitted to *Polymer*, June 1991.
(29) Eisenberg, A.; Hird, B.; Moore, R. B. *Macromolecules* **1990**, *23*, 4098.